CMS Physics Analysis Summary

Contact: cms-pag-conveners-top@cern.ch 2018/07/04

Measurement of the top quark mass in the all-jets final state at $\sqrt{s} = 13$ TeV

The CMS Collaboration

Abstract

A top quark mass measurement is performed using 35.9 fb^{-1} of LHC proton-proton collision data collected with the CMS detector at $\sqrt{s} = 13$ TeV in 2016. The measurement uses the $\mathrm{t\bar{t}}$ all-jets final state, which comprises a total of six jets. A kinematic fit is performed to reconstruct the decay of the $\mathrm{t\bar{t}}$ system and suppress QCD multijet background. By means of the ideogram method, the top quark mass is determined, simultaneously constraining an additional jet energy scale factor (JSF). The result of $172.34 \pm 0.20\,\text{(stat+JSF)} \pm 0.76\,\text{(syst)}$ GeV for the top quark mass is in good agreement with previous measurements in the same and different final states.

1 Introduction

The top quark is the heaviest known fundamental particle and its mass m_t is an important parameter of the standard model (SM) of particle physics. Precise measurements of m_t can be used to test the consistency of the SM [1–3] and search for new physics. Since the top quark dominates the higher order corrections to the Higgs boson mass, m_t can also be used to put constraints on the stability of the electroweak vacuum [4, 5].

At the CERN LHC, top quarks are predominantly produced in quark-antiquark pairs ($t\bar{t}$) through the gluon fusion process and almost exclusively decay to a b quark and a W boson. Each $t\bar{t}$ event can be classified by the decays of the daughter W bosons. In the all-jets decay channel, only events where both W bosons decay further into two $q\bar{q}'$ pairs are considered.

This document presents a measurement of m_t obtained in the $t\bar{t}$ all-jets decay channel using data taken in 2016 by the CMS experiment at a center-of-mass energy of 13 TeV corresponding to an integrated luminosity of 35.9 fb^{-1}. The two bottom quarks and the four light quarks from the $t\bar{t}$ decay are required to be well separated in the laboratory frame of reference, hence the experimental signature is characterized by six jets in the detector.

Although this final state provides the largest branching fraction of all top quark pair decays, the measurement of m_t in this channel is particularly challenging due to the large background from QCD multijet production. A kinematic fit of the decay products to a $t\bar{t}$ hypothesis is employed to effectively separate signal from background events.

The top quark mass is extracted using the ideogram method [6, 7], which uses likelihood functions for each event that depend on the top quark mass only or on both the top quark mass and an additional jet energy scale factor (JSF). In the second case, the invariant mass of the two jets associated with the $W \to q\bar{q}'$ decay serves as an observable in the likelihood functions to estimate the JSF directly.

The previous result by the CMS Collaboration in this decay channel using similar techniques as in this study, but with data at $\sqrt{s} = 8$ TeV, obtained a top quark mass of [8]

$$172.32 \pm 0.25\,(\text{stat+JSF}) \pm 0.59\,(\text{syst})\,\text{GeV}.$$

The ATLAS Collaboration has published a measurement using the same final state with $\sqrt{s} = 7$ TeV data [9]. Combining the results of several measurements using different final states, the ATLAS and CMS Collaborations reported values of $m_t = 172.84 \pm 0.70$ GeV [10] and $m_t = 172.44 \pm 0.49$ GeV [8], respectively.

A first top quark mass measurement using proton-proton (pp) collision data at $\sqrt{s} = 13$ TeV in the lepton+jets channel resulted in $m_t = 172.25 \pm 0.08\,(\text{stat+JSF}) \pm 0.62\,(\text{syst})$ GeV [11], based on the dataset collected in 2016, which is also used in this analysis.

2 Event selection and simulation

Jets are clustered from particle flow (PF) [12] objects with the anti-k_t algorithm and a distance parameter of 0.4 [13–15], excluding charged hadron tracks not originating from the primary collision vertex. Only jets with $p_T > 30$ GeV reconstructed within $|\eta| < 2.4$ are used in the analysis. For the identification of jets originating from the hadronization of b quarks the combined secondary vertex algorithm (CSVv2) b tagger is used [16]. The chosen working point provides an identification efficiency of approximately 50% with a probability of misidentifying a light-flavor (uds) or gluon jet of approximately 0.1%. The hadronic activity is defined as the

scalar sum of all jet transverse momenta

$$H_{\mathrm{T}} \equiv \sum_{\text{jets}} p_{\mathrm{T}}.$$

Data events are selected by a High Level Trigger (HLT) requiring the presence of at least six PF jets with $p_{\mathrm{T}} > 40\,\mathrm{GeV}$ and $H_{\mathrm{T}} > 450\,\mathrm{GeV}$. Additionally, at least one jet is required to be b-tagged.

In the offline selection, an event needs to contain a well reconstructed vertex localized within 24 cm in z direction and 2 cm in x-y direction around the nominal interaction point. Selected events are required to contain at least six jets, at least two of which have to be tagged as b jets. The sixth jet (jet_6), ordered in p_{T}, needs to have a transverse momentum of $p_{\mathrm{T}}(\mathrm{jet}_6) > 40\,\mathrm{GeV}$ and $H_{\mathrm{T}} > 450\,\mathrm{GeV}$ is required. The two b jets have to be separated in $\Delta R = \sqrt{\Delta\phi^2 + \Delta\eta^2}$ by $\Delta R(\mathrm{b\bar{b}}) > 2.0$.

Simulation of the $\mathrm{t\bar{t}}$ signal assuming a mass of 172.5 GeV is performed using the POWHEG v2 [17–20] matrix-element (ME) generator in next-to-leading order perturbative QCD. For the parton distribution function (PDF) the NNPDF3.0 NLO set [21] is used with the strong coupling constant $\alpha_S = 0.118$. This is one of the first PDF sets including total $\mathrm{t\bar{t}}$ cross-section measurements from ATLAS and CMS at $\sqrt{s} = 7$ and 8 TeV as input. The parton shower and hadronization are handled by PYTHIA 8.219 [22] using the CUETP8M2T4 tune [23, 24] and GEANT4 is used to simulate the response of the CMS detector [25]. The simulated signal sample is normalized to the integrated luminosity of the data sample using the next-to-next-to-leading order cross section of $\sigma_{\mathrm{t\bar{t}}} = 832\,\mathrm{pb}$ [26]. In addition to the default sample, six further samples are used assuming top quark masses of 166.5, 169.5, 171.5, 173.5, 175.5, and 178.5 GeV.

For simulated events, an HLT emulation is used. The residual differences in the trigger efficiency between data and simulation are corrected by applying scale factors to the simulated events. These are obtained by measuring the trigger efficiency with respect to a reference H_{T}-trigger for both data and simulation. The parametrized ratio as a function of $p_{\mathrm{T}}(\mathrm{jet}_6)$ and H_{T} is used to reweight the simulated events. Additional pp collisions (pileup) are included in the simulated events. These are reweighted to match the pileup distribution in data. Furthermore, corrections to the jet energy scale and resolution, as well as to the b-tagging efficiency, are applied.

3 Kinematic fit and background estimation

To improve the resolution of the top quark mass and decrease the background contribution, a kinematic fit is applied. It exploits the known topology of the signal events, i.e., pair production of a heavy particle and anti-particle, each decaying to Wb with $\mathrm{W} \to \mathrm{q\bar{q}}'$. The three-momenta of the jets are varied and the minimum of

$$\chi^2 = \sum_{j \in \text{jets}} \left[\frac{\left(p_{\mathrm{T}_j}^{\text{reco}} - p_{\mathrm{T}_j}^{\text{fit}}\right)^2}{\sigma^2_{p_{\mathrm{T}j}}} + \frac{\left(\eta_j^{\text{reco}} - \eta_j^{\text{fit}}\right)^2}{\sigma^2_{\eta_j}} + \frac{\left(\phi_j^{\text{reco}} - \phi_j^{\text{fit}}\right)^2}{\sigma^2_{\phi_j}} \right]$$

is determined while constraining the invariant mass of the jets assigned to each W-boson decay to $m_{\mathrm{W}} = 80.4\,\mathrm{GeV}$. As an additional constraint, the two top quark candidates are required to have equal invariant masses.

All possible parton-jet assignments are tested using the leading six jets in the event, but only b-tagged jets are used as b candidates and equivalent choices (e.g. swapping the two jets originating from one W boson) are not considered separately. Of the remaining 12 possibilities only the assignment yielding the smallest χ^2 is used in the following. The χ^2 value can be used as a goodness-of-fit measure (gof). For three degrees of freedom, it is translated into a p-value of

$$P_{\text{gof}} \equiv 1 - \text{erf}\left(\sqrt{\frac{\chi^2}{2}}\right) + \sqrt{\frac{2\chi^2}{\pi}} \text{e}^{-\chi^2/2}.$$

Events are required to fulfill $P_{\text{gof}} > 0.1$ for the best assignment. The P_{gof} distribution is displayed in Fig. 1 (right).

In simulation, event generator information can be used to validate the correct assignment of the reconstructed jets to the top quark decay products. Events are classified accordingly as *correct* or *wrong* permutations. A parton-jet assignment is considered correct if the jets can be matched unambiguously to the right partons within $\Delta R < 0.3$. Wrong permutations can occur due to a wrong parton-jet assignment yielding the smallest χ^2 or jets being out of acceptance, not being reconstructed, or failing the identification requirements.

Requiring $P_{\text{gof}} > 0.1$ increases the fraction of correct permutations from 6% to 51%. The fitted top quark mass ($m_{\text{t}}^{\text{fit}}$) is calculated as the invariant mass of the corresponding jets returned by the kinematic fit. Compared to the mass calculated from the originally reconstructed jets the mass resolution is improved from 14.0 GeV to 8.8 GeV for the correct parton-jet assignments, where in both cases the same events passing the $P_{\text{gof}} > 0.1$ are used.

The $\Delta R(\text{b}\bar{\text{b}}) > 2.0$ and $P_{\text{gof}} > 0.1$ requirements greatly reduce the background from QCD multijet production, but a significant number of events enters the signal selection owing to the large production cross section. These events are fulfilling the goodness-of-fit criterion due to combinatorial chance, but not due to an underlying decay topology. Therefore, it is assumed that b jets can be exchanged with light jets for the background estimation, which is purely data driven.

For the background estimation the same selection as for the signal is applied as described above, but instead of requiring two b-tagged jets, events with exactly zero b-tagged jets are used. For this veto a very loose working point is used for the b tagger to exclude signal contamination of $\text{t}\bar{\text{t}}$ events in this QCD-enriched sample. A prescaled trigger similar to the signal trigger is used for this selection, which is not requiring the presence of b jets. The kinematic fit is applied as before, but here any of the six light jets can be assigned to the partons originating from the W decays, as well as to the partons serving as b quarks, leading to 90 possible permutations that have to be evaluated. This method allows the determination of the kinematic shapes of the background, but the normalization is unknown. In the following plots the background is normalized to the difference of the integrals of the data and expected signal distributions. This sample contains approximately five times the number of expected background events, so it provides a good statistical precision.

The final selected data set consists of 10799 events with a signal purity of 75%. Figure 1 shows the distributions of the separation of the two b jets $\Delta R(\text{b}\bar{\text{b}})$ and the goodness-of-fit probability P_{gof} in data compared to the background estimate and $\text{t}\bar{\text{t}}$ simulation. For the $\text{t}\bar{\text{t}}$ signal, correct and wrong parton-jet assignments are shown separately. The corresponding distributions of the fitted top quark mass $m_{\text{t}}^{\text{fit}}$ and the reconstructed W boson mass $m_{\text{W}}^{\text{reco}}$, calculated from the originally reconstructed jets, are shown in Fig. 2. These two quantities are the ones used in the top quark mass extraction described in the following.

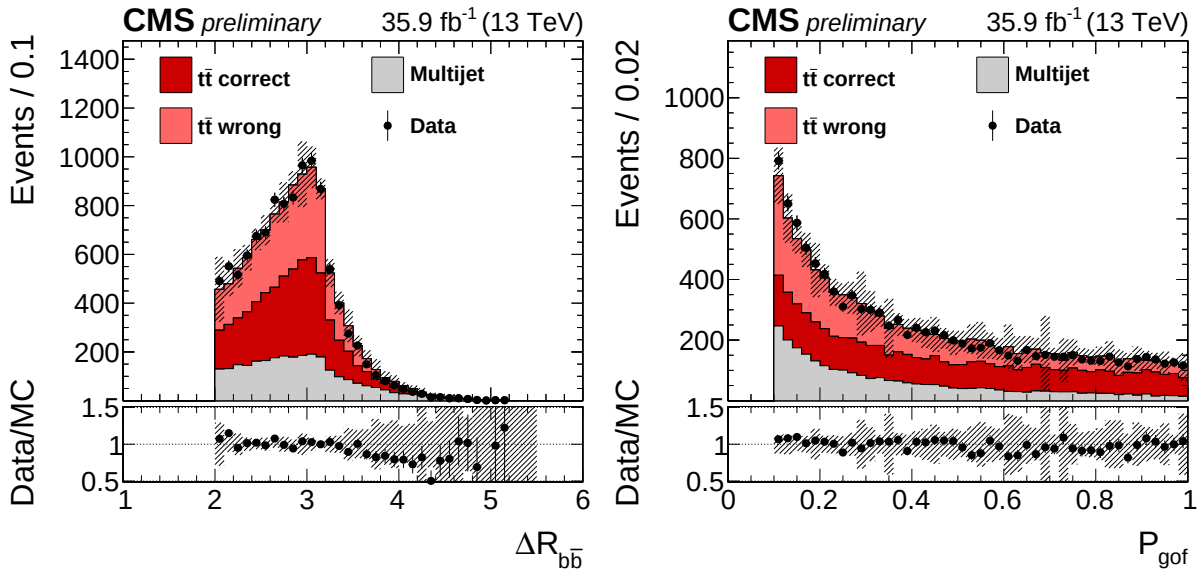

Figure 1: The $\Delta R(\mathrm{b\bar{b}})$ (left) and P_{gof} (right) distributions of data compared to signal simulation and the multijet background estimate. The hashed bands represent the total uncertainty of the prediction.

4 Ideogram method

For the extraction of the top quark mass m_{t} the ideogram method is used [6, 7]. Simultaneously, a jet scale factor (JSF) is determined that is used on top of the standard CMS jet energy calibration [8] to reduce the corresponding systematic uncertainty. The distributions of the top quark mass $m_{\mathrm{t}}^{\mathrm{fit}}$ obtained from the kinematic fit and the average reconstructed W boson mass $m_{\mathrm{W}}^{\mathrm{reco}}$ are used as estimators in a combined fit.

The likelihood

$$\begin{aligned}\mathcal{L}\left(m_{\mathrm{t}}, \mathrm{JSF}\right) &= P\left(\mathrm{sample}|m_{\mathrm{t}}, \mathrm{JSF}\right) \\ &= \prod_{\mathrm{events}} P\left(\mathrm{event}|m_{\mathrm{t}}, \mathrm{JSF}\right) \\ &= \prod_{\mathrm{events}} P\left(m_{\mathrm{t}}^{\mathrm{fit}}, m_{\mathrm{W}}^{\mathrm{reco}}|m_{\mathrm{t}}, \mathrm{JSF}\right)\end{aligned}$$

is maximized, yielding the best-fit values for m_{t} and JSF. A prior probability for the JSF can be incorporated by maximizing

$$P(\mathrm{JSF}) \cdot P\left(\mathrm{sample}|m_{\mathrm{t}}, \mathrm{JSF}\right)$$

instead. Treating $m_{\mathrm{t}}^{\mathrm{fit}}$ and $m_{\mathrm{W}}^{\mathrm{reco}}$ as uncorrelated, the probability $P\left(m_{\mathrm{t}}^{\mathrm{fit}}, m_{\mathrm{W}}^{\mathrm{reco}}|m_{\mathrm{t}}, \mathrm{JSF}\right)$ factorizes into

$$\begin{aligned}P\left(m_{\mathrm{t}}^{\mathrm{fit}}, m_{\mathrm{W}}^{\mathrm{reco}}|m_{\mathrm{t}}, \mathrm{JSF}\right) &= f_{\mathrm{sig}} \cdot P\left(m_{\mathrm{t}}^{\mathrm{fit}}, m_{\mathrm{W}}^{\mathrm{reco}}|m_{\mathrm{t}}, \mathrm{JSF}\right) \\ &\quad + \left(1 - f_{\mathrm{sig}}\right) \cdot P_{\mathrm{bkg}}\left(m_{\mathrm{t}}^{\mathrm{fit}}, m_{\mathrm{W}}^{\mathrm{reco}}\right) \\ &= f_{\mathrm{sig}} \cdot \sum_{j} f_j P_j\left(m_{\mathrm{t}}^{\mathrm{fit}}|m_{\mathrm{t}}, \mathrm{JSF}\right) \cdot P_j\left(m_{\mathrm{W}}^{\mathrm{reco}}|m_{\mathrm{t}}, \mathrm{JSF}\right) \\ &\quad + \left(1 - f_{\mathrm{sig}}\right) \cdot P_{\mathrm{bkg}}\left(m_{\mathrm{t}}^{\mathrm{fit}}\right) \cdot P_{\mathrm{bkg}}\left(m_{\mathrm{W}}^{\mathrm{reco}}\right)\end{aligned}$$

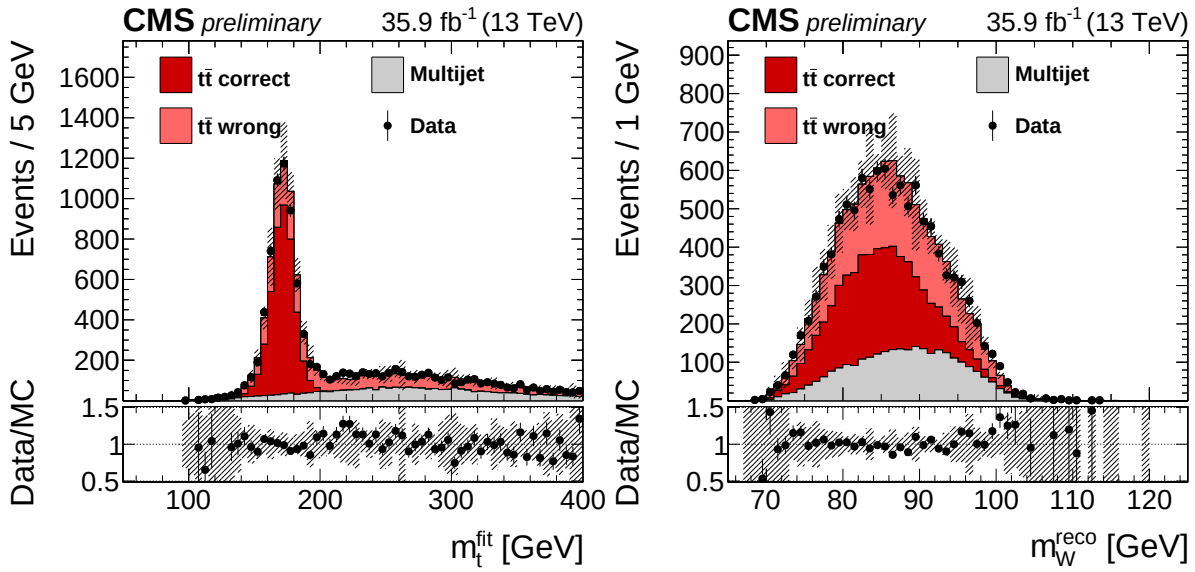

Figure 2: The fitted top quark mass (left) and reconstructed W boson mass (right) distributions of data compared to signal simulation and the multijet background estimate. The shown reconstructed W boson mass is the average of both W bosons in the event. The hashed bands represent the total uncertainty of the prediction.

where f_j with $j \in \{\text{correct}, \text{wrong}\}$ is the relative fraction of the different permutation cases and f_{sig} the signal fraction.

The probability densities $P_j\left(m_{\text{t}}^{\text{fit}}|m_{\text{t}}, \text{JSF}\right)$ and $P_j\left(m_{\text{W}}^{\text{reco}}|m_{\text{t}}, \text{JSF}\right)$ for the signal are described by analytic functions parametrized in m_{t} and JSF. For the determination of the parameters, a simultaneous fit to simulated samples for seven different generated top quark masses $m_{\text{t}}^{\text{gen}}$ and five different input JSF values is used. The background is described by a spline interpolation independent of m_{t} and JSF.

Three variations of a maximum likelihood fit are performed to extract the top quark mass. In the 1D analysis, the JSF is fixed to unity (prior probability $\propto \delta(1)$), i.e., the standard CMS jet energy calibration. For the 2D analysis the JSF is completely free in the maximum likelihood fit. The signal fraction and correct permutation fraction are free parameters in both cases. The hybrid method is a weighted combination of both approaches, corresponding to a Gaussian constraint of the JSF around unity. The prior probability reflects the knowledge from the standard CMS jet energy corrections and is described by a Gaussian probability density.

To calibrate the mass extraction method, pseudo-experiments are performed for seven different generated values of $m_{\text{t}}^{\text{gen}}$ and three input JSF values. The extracted m_{t} and JSF values are compared to the input values and the residual slope is used as calibration. The residual biases after the calibration are shown in Fig. 3 for pseudo-experiments for different JSF and $m_{\text{t}}^{\text{gen}}$ values. Neither a significant residual offset nor slope are observed.

5 Systematic uncertainties

A summary of the systematic uncertainty sources is shown in Table 1. These values are obtained from pseudo-experiments using signal samples with variations of the individual systematic uncertainty sources. In the following, details for the determination of the most important uncertainties are given. Most systematic uncertainty sources are shifted by ± 1 standard devia-

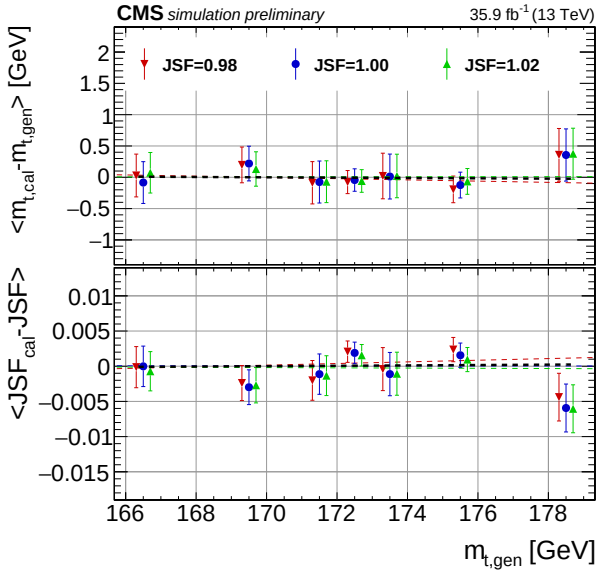

Figure 3: Difference of extracted and generated top quark masses and JSFs for different input masses and JSFs after the calibration.

tion and the absolute value of the largest resulting shifts in m_t and JSF are quoted as systematic uncertainties for the measurement. For some uncertainties, different models are compared as described individually. The maximum of the statistical uncertainty on the observed shift and the shift itself is used as the systematic uncertainty.

Method calibration: The quadratic sum of statistical uncertainty and residual biases (see Fig. 3) after the calibration is used as systematic uncertainty.

JECs: Jet energies are scaled up and down according the p_T- and η-dependent data/simulation uncertainties [27]. The correlation groups follow the recommendations documented in Ref. [28].

Jet energy resolution: Since the jet energy resolution measured in data is worse than in simulation, the simulation is modified to correct for the difference [27]. The jet energy resolution in the simulation is varied up and down within the uncertainty.

b tagging: The p_T-dependent uncertainty of the b-tagging efficiencies and misidentification rates of the CSV b tagger [16] is taken into account by reweighting the simulated events accordingly.

Pileup: For the uncertainty in the determination of the number of pileup events and the reweighting procedure, the inelastic pp cross section used in the determination is varied by $\pm 4.6\%$.

Background: An uncertainty of the background prediction is obtained by applying the method to simulation and comparing the obtained estimate to the direct simulation. A linear fit to the ratio is consistent with unity. The slope is varied up and down within its uncertainty and used to reweight the events used for the background PDF determination.

Trigger: To estimate the uncertainty of the trigger selection, the data/simulation scale factor described in Section 2 is omitted. Additionally a base trigger requiring the presence of one muon is used to derive the correction factor. The maximum of the observed shifts with respect to the nominal correction is quoted as uncertainty.

Table 1: List of systematic uncertainties for the all-jets channel. The signs of the shifts correspond to the +1 standard deviation variation of the systematic uncertainty source. For linear sums of uncertainty groups, the relative signs have been considered.

	2D		1D	hybrid	
	δm_t^{2D} [GeV]	δJSF^{2D} [%]	δm_t^{1D} [GeV]	δm_t^{hyb} [GeV]	δJSF^{hyb} [%]
Experimental uncertainties					
Method calibration	0.06	0.2	0.06	0.06	0.2
JEC (quad. sum)	0.18	0.3	0.73	0.15	0.2
- Intercalibration	−0.04	−0.1	+0.12	−0.04	−0.1
- MPFInSitu	−0.03	−0.0	+0.22	+0.08	+0.1
- Uncorrelated	−0.17	−0.3	+0.69	+0.12	+0.2
Jet energy resolution	−0.12	+0.4	+0.18	−0.03	+0.3
b tagging	0.02	0.0	0.01	0.02	0.0
Pileup	−0.06	+0.1	+0.00	−0.04	+0.1
Background	0.10	0.1	0.03	0.07	0.1
Trigger	+0.04	−0.1	−0.04	+0.02	−0.1
Modeling of hadronization					
JEC Flavor (linear sum)	−0.35	+0.1	−0.31	−0.34	+0.0
- light quarks (uds)	+0.10	−0.1	−0.01	+0.07	−0.1
- charm	+0.03	−0.0	−0.01	+0.02	−0.0
- bottom	−0.29	−0.0	−0.29	−0.29	−0.0
- gluon	−0.19	+0.2	+0.03	−0.13	+0.2
b jet modeling (quad. sum)	0.09	0.0	0.09	0.09	0.0
- b frag. Bowler-Lund	−0.07	+0.0	−0.07	−0.07	+0.0
- b frag. Peterson	−0.05	+0.0	−0.04	−0.05	+0.0
- semi-leptonic B decays	−0.03	−0.0	−0.03	−0.03	−0.0
Modeling of perturbative QCD					
PDF	0.01	0.0	0.01	0.01	0.0
Ren. and fact. scale	0.05	0.0	0.04	0.04	0.0
ME/PS matching	$+0.32 \pm 0.20$	−0.3	-0.05 ± 0.14	$+0.24 \pm 0.18$	−0.2
ME generator	$+0.29 \pm 0.34$	+0.1	$+0.36 \pm 0.24$	$+0.31 \pm 0.30$	+0.1
ISR PS scale	$+0.17 \pm 0.17$	−0.2	$+0.13 \pm 0.12$	$+0.12 \pm 0.14$	−0.1
FSR PS scale	$+0.22 \pm 0.12$	−0.2	$+0.11 \pm 0.08$	$+0.18 \pm 0.11$	−0.1
Top quark p_T	+0.03	−0.0	+0.02	+0.03	−0.0
Modeling of soft QCD					
Underlying event	$+0.16 \pm 0.19$	−0.3	-0.07 ± 0.14	$+0.10 \pm 0.17$	−0.2
Early resonance decays	$+0.02 \pm 0.28$	+0.4	$+0.38 \pm 0.19$	$+0.13 \pm 0.24$	+0.3
CR modeling (max. shift)	$+0.41 \pm 0.29$	−0.4	-0.43 ± 0.20	-0.36 ± 0.25	−0.3
- "gluon move" (ERD on)	$+0.41 \pm 0.29$	−0.4	$+0.10 \pm 0.20$	$+0.32 \pm 0.25$	−0.3
- "QCD inspired" (ERD on)	-0.32 ± 0.29	−0.1	-0.43 ± 0.20	-0.36 ± 0.25	−0.1
Total systematic	**0.88**	**1.0**	**1.10**	**0.76**	**0.7**
Statistical (expected)	0.21	0.2	0.16	0.20	0.1
Total (expected)	**0.91**	**1.0**	**1.11**	**0.79**	**0.7**

JEC Flavor: The difference of the Lund string fragmentation and the cluster fragmentation is evaluated comparing PYTHIA 6.4 [29] and HERWIG++ 2.4 [30]. The jet energy response is compared separately for each jet flavor [27]. Uncertainties for jets from different quark flavors and gluons are added linearly, allowing to take into account possible differences

between the measured JSF, which is mainly sensitive to light quarks and gluons, and the b jet energy scale.

b **jet modeling:** The uncertainty associated with the fragmentation of b quarks is split into three components. The Bowler–Lund fragmentation function is varied within its uncertainties as determined by the ALEPH and DELPHI collaborations [31, 32]. As an alternative model of the fragmentation into b hadrons, the Peterson fragmentation function is used and the difference to the result using the Bowler–Lund fragmentation function is assigned as an uncertainty. The third uncertainty source taken into account is the semileptonic b hadron branching fraction, which is varied by -0.45% and $+0.77\%$, motivated by measurements of B^0/B^+decays and the corresponding uncertainties [33].

PDF: The 100 PDF replicas of the NNPDF3.0 NLO ($\alpha_s = 0.118$) set are used to repeat the analysis [21]. The variance of the results is used to determine the PDF uncertainty. In addition, α_s is scaled to 0.117 and 0.119. The maximum of the PDF uncertainty and the α_s variations is quoted as uncertainty.

Renormalization and factorization scales: Renormalization and factorization scales for the matrix-element calculation are used that are multiplied independently from each other and simultaneously by factors of 0.5 and 2 compared to the default values. This is achieved by reweighting simulated events appropriately. The quoted uncertainty corresponds to the envelope of the resulting shifts.

ME/PS matching: The matching of the POWHEG matrix elements to the PYTHIA parton showers is varied by shifting the parameter $h_{\text{damp}} = 1.58^{+0.66}_{-0.59}$ [24] within the uncertainties. The jet response $\frac{{p_T}^{\text{reco}}}{{p_T}^{\text{gen}}}({p_T}^{\text{gen}})$ is rescaled in the variation samples to reproduce the response observed in the default sample.

ME generator: Instead of using POWHEG v2 as matrix-element generator, the MADGRAPH5_aMC@NLO generator with the FxFx matching scheme is used [34, 35].

ISR PS scale: For the initial-state radiation (ISR), the parton shower (PS) scale is varied in PYTHIA. The ISR PS scale is multiplied by 2 and 0.5 in dedicated samples.

FSR PS scale: The PS scale used for final-state radiation (FSR) is scaled up by $\sqrt{2}$ and down by $1/\sqrt{2}$ [23], affecting the fragmentation and hadronization, as well additional jet emission. The jet response is rescaled in the variation samples to reproduce the response observed in the default sample.

Top quark p_T: Recent calculations suggest that the top quark p_T spectrum is strongly affected by next-to-next-to-leading-order effects [36]. Therefore, the top quark p_T in simulation is varied to match the distribution measured by CMS [37, 38] and its effect on the measurement is quoted as a systematic uncertainty.

Underlying event: Underlying event measurements have been used to tune PYTHIA parameters describing non-perturbative QCD effects [23, 24]. The parameters of the tune are varied within their uncertainties.

Early resonance decays: Color reconnection (CR) modeling introduces systematic uncertainties which are estimated by comparing different CR models and settings. In the default sample the top quark decay products are not included in the CR process. This setting is compared to the case of including the decay products by enabling early resonance decays (ERD) in PYTHIA 8.

CR modeling: In addition to the default model used in PYTHIA 8, two alternative CR models are used, namely a model with string formation beyond leading color ("QCD inspired") [39] and a model allowing the gluons to be moved to another string ("gluon move") [40]. Underlying event measurements are used to tune the parameters of all models [23, 24]. The largest shifts of the variations are assigned as the CR uncertainty.

This approach, as well as the early resonance decay variation, is new with respect to the Run 1 results, because these color-reconnection models are newly available in PYTHIA 8. The new models have first been used to evaluate the m_t uncertainty due to color reconnection in Ref. [11].

6 Results

For the 2D fit using the 10799 $t\bar{t}$ all-jets candidate events, the extracted parameters are

$$m_t^{2D} = 172.43 \pm 0.22\,(\text{stat+JSF}) \pm 0.88\,(\text{syst})\,\text{GeV and}$$
$$\text{JSF}^{2D} = 0.996 \pm 0.002\,(\text{stat}) \pm 0.010\,(\text{syst}).$$

The corresponding 1D and hybrid fits yield

$$m_t^{1D} = 172.13 \pm 0.17\,(\text{stat}) \pm 1.10\,(\text{syst})\,\text{GeV},$$
$$m_t^{hyb} = 172.34 \pm 0.20\,(\text{stat+JSF}) \pm 0.76\,(\text{syst})\,\text{GeV, and}$$
$$\text{JSF}^{hyb} = 0.997 \pm 0.002\,(\text{stat}) \pm 0.007\,(\text{syst}).$$

The hybrid measurement of $172.34 \pm 0.20\,(\text{stat+JSF}) \pm 0.43\,(\text{CR+ERD}) \pm 0.63\,(\text{syst})\,\text{GeV}$ is the main result of this analysis, since it is constructed to provide the lowest uncertainty. The color reconnection and early resonance decay parts are separated from the rest of the systematic uncertainties here. Due to the larger data sample used in this analysis, the statistical uncertainty is reduced with respect to the result of $m_t = 172.32 \pm 0.25\,(\text{stat+JSF}) \pm 0.59\,(\text{syst})\,\text{GeV}$ obtained at $\sqrt{s} = 8\,\text{TeV}$. The systematic uncertainty is increased with respect to the Run 1 result, mainly because of the availability of more sophisticated color-reconnection model variations in PYTHIA 8. These new models have first been used to evaluate the m_t uncertainty due to color reconnection in Ref. [11], where the same increase in systematic uncertainty with respect to the Run 1 result is observed. This is the first time a NLO $t\bar{t}$ simulation has been employed to calibrate a direct top quark mass measurement in the all-jets final state.

7 Summary

In this study, a measurement of the top quark mass using events with at least six jets in the final state has been presented. The analyzed data was collected with the CMS experiment in pp collisions at $\sqrt{s} = 13\,\text{TeV}$. This data sample corresponds to an integrated luminosity of $35.9\,\text{fb}^{-1}$ and contains 10799 candidate events after the event selection. The kinematic properties in each event are reconstructed using a constrained fit, assuming a $t\bar{t}$ hypothesis, which allowed to suppress the dominant QCD multijet background and improve the mass resolution.

The top quark mass and an additional jet energy scale factor were extracted using the ideogram method, which uses the likelihood of the top quark mass and jet scale factor in each event to determine these parameters. The resulting top quark mass is measured to be $172.34 \pm 0.20\,(\text{stat+JSF}) \pm 0.43\,(\text{CR+ERD}) \pm 0.63\,(\text{syst})\,\text{GeV} = 172.34 \pm 0.20\,(\text{stat+JSF}) \pm 0.76\,(\text{syst})\,\text{GeV}$.

This is in good agreement with the previous CMS results at $\sqrt{s} = 7$ and 8 TeV [8], as well as with the result in the lepton+jets channel at $\sqrt{s} = 13$ TeV [11]. The quoted modeling uncertainties are increased with respect to previous results at lower center-of-mass energies due to the utilization of alternative color-reconnection models which have not been available previously.

References

[1] Tevatron Electroweak Working Group, CDF, DELPHI, SLD Electroweak and Heavy Flavour Groups, ALEPH, LEP Electroweak Working Group, SLD, OPAL, D0, L3 Collaboration, "Precision Electroweak Measurements and Constraints on the Standard Model", arXiv:1012.2367.

[2] M. Baak et al., "The Electroweak Fit of the Standard Model after the Discovery of a New Boson at the LHC", *Eur. Phys. J. C* **72** (2012) 2205, doi:10.1140/epjc/s10052-012-2205-9, arXiv:1209.2716.

[3] M. Baak et al., "The global electroweak fit at NNLO and prospects for the LHC and ILC", *Eur. Phys. J. C* **74** (2014) 3046, doi:10.1140/epjc/s10052-014-3046-5, arXiv:1407.3792.

[4] G. Degrassi et al., "Higgs mass and vacuum stability in the standard model at NNLO", *JHEP* **08** (2012) 1, doi:10.1007/JHEP08(2012)098, arXiv:1205.6497.

[5] F. Bezrukov, M. Y. Kalmykov, B. A. Kniehl, and M. Shaposhnikov, "Higgs boson mass and new physics", *JHEP* **10** (2012) 140, doi:10.1007/JHEP10(2012)140, arXiv:1205.2893.

[6] DELPHI Collaboration, "Measurement of the mass and width of the W boson in e^+e^- collisions at $\sqrt{s}$ = 161 – 209 GeV", *Eur. Phys. J. C* **55** (2008) 1, doi:10.1140/epjc/s10052-008-0585-7, arXiv:0803.2534.

[7] CMS Collaboration, "Measurement of the top-quark mass in $t\bar{t}$ events with lepton+jets final states in pp collisions at $\sqrt{s} = 7$ TeV", *JHEP* **12** (2012) 105, doi:10.1007/JHEP12(2012)105, arXiv:1209.2319.

[8] CMS Collaboration, "Measurement of the top quark mass using proton-proton data at $\sqrt{s}$ = 7 and 8 TeV", *Phys. Rev. D* **93** (2016) 072004, doi:10.1103/PhysRevD.93.072004, arXiv:1509.04044.

[9] ATLAS Collaboration, "Measurement of the top-quark mass in the fully hadronic decay channel from ATLAS data at $\sqrt{s} = 7$ TeV", *Eur. Phys. J. C* **75** (2015) 158, doi:10.1140/epjc/s10052-015-3373-1, arXiv:1409.0832.

[10] ATLAS Collaboration, "Measurement of the top quark mass in the $t\bar{t} \to$ dilepton channel from $\sqrt{s} = 8$ TeV ATLAS data", *Phys. Lett. B* **761** (2016) 350, doi:10.1016/j.physletb.2016.08.042, arXiv:1606.02179.

[11] CMS Collaboration, "Measurement of the top quark mass with lepton+jets final states using pp collisions at $\sqrt{s} = 13$ TeV", (2018). arXiv:1805.01428. Submitted to *Eur. Phys. J. C.*

[12] CMS Collaboration, "Particle-flow reconstruction and global event description with the CMS detector", *JINST* **12** (2017) P10003, doi:10.1088/1748-0221/12/10/P10003, arXiv:1706.04965.

[13] M. Cacciari and G. P. Salam, "Dispelling the N^3 myth for the k_t jet-finder", *Phys. Lett. B* **641** (2006) 57, doi:10.1016/j.physletb.2006.08.037, arXiv:hep-ph/0512210.

[14] M. Cacciari, G. P. Salam, and G. Soyez, "The anti-k_t jet clustering algorithm", *JHEP* **04** (2008) 063, doi:10.1088/1126-6708/2008/04/063, arXiv:0802.1189.

[15] M. Cacciari, G. P. Salam, and G. Soyez, "FastJet user manual", *Eur. Phys. J. C* **72** (2012) 1896, doi:10.1140/epjc/s10052-012-1896-2, arXiv:1111.6097.

[16] CMS Collaboration, "Identification of heavy-flavour jets with the CMS detector in pp collisions at 13 TeV", *JINST* **13** (2018), no. 05, P05011, doi:10.1088/1748-0221/13/05/P05011, arXiv:1712.07158.

[17] P. Nason, "A new method for combining NLO QCD with shower Monte Carlo algorithms", *JHEP* **11** (2004) 040, doi:10.1088/1126-6708/2004/11/040, arXiv:hep-ph/0409146.

[18] S. Frixione, P. Nason, and C. Oleari, "Matching NLO QCD computations with parton shower simulations: the POWHEG method", *JHEP* **11** (2007) 070, doi:10.1088/1126-6708/2007/11/070, arXiv:0709.2092.

[19] S. Alioli, P. Nason, C. Oleari, and E. Re, "A general framework for implementing NLO calculations in shower Monte Carlo programs: the POWHEG BOX", *JHEP* **06** (2010) 043, doi:10.1007/JHEP06(2010)043, arXiv:1002.2581.

[20] J. M. Campbell, R. K. Ellis, P. Nason, and E. Re, "Top-pair production and decay at NLO matched with parton showers", *JHEP* **04** (2015) 114, doi:10.1007/JHEP04(2015)114, arXiv:1412.1828.

[21] NNPDF Collaboration, "Parton distributions for the LHC Run II", *JHEP* **04** (2015) 040, doi:10.1007/JHEP04(2015)040, arXiv:1410.8849.

[22] T. Sjostrand, S. Mrenna, and P. Z. Skands, "A Brief Introduction to PYTHIA 8.1", *Comput. Phys. Commun.* **178** (2008) 852, doi:10.1016/j.cpc.2008.01.036, arXiv:0710.3820.

[23] P. Skands, S. Carrazza, and J. Rojo, "Tuning PYTHIA 8.1: the Monash 2013 Tune", *Eur. Phys. J. C* **74** (2014) 3024, doi:10.1140/epjc/s10052-014-3024-y, arXiv:1404.5630.

[24] CMS Collaboration, "Investigations of the impact of the parton shower tuning in PYTHIA 8 in the modelling of $\mathrm{t\bar{t}}$ at $\sqrt{s} = 8$ and 13 TeV", CMS Physics Analysis Summary CMS-PAS-TOP-16-021, 2016.

[25] GEANT4 Collaboration, "GEANT4—a simulation toolkit", *Nucl. Instrum. Meth. A* **506** (2003) 250, doi:10.1016/S0168-9002(03)01368-8.

[26] M. Czakon and A. Mitov, "Top++: A Program for the Calculation of the Top-Pair Cross-Section at Hadron Colliders", *Comput. Phys. Commun.* **185** (2014) 2930, doi:10.1016/j.cpc.2014.06.021, arXiv:1112.5675.

[27] CMS Collaboration, "Jet energy scale and resolution in the CMS experiment in pp collisions at 8 TeV", *JINST* **12** (2017) P02014, doi:10.1088/1748-0221/12/02/P02014, arXiv:1607.03663.

[28] ATLAS and CMS Collaborations, "Jet energy scale uncertainty correlations between ATLAS and CMS at 8 TeV", ATL-PHYS-PUB-2015-049, CMS-PAS-JME-15-001, CERN, 2015.

[29] T. Sjöstrand, S. Mrenna, and P. Skands, "PYTHIA 6.4 physics and manual", *JHEP* **05** (2006) 026, doi:10.1088/1126-6708/2006/05/026, arXiv:hep-ph/0603175.

[30] M. Bähr et al., "Herwig++ physics and manual", *Eur. Phys. J. C* **58** (2008) 639, doi:10.1140/epjc/s10052-008-0798-9, arXiv:0803.0883.

[31] DELPHI Collaboration, "A study of the b-quark fragmentation function with the DELPHI detector at LEP I and an averaged distribution obtained at the Z Pole", *Eur. Phys. J. C* **71** (2011) 1557, doi:10.1140/epjc/s10052-011-1557-x, arXiv:1102.4748.

[32] ALEPH Collaboration, "Study of the fragmentation of b quarks into B mesons at the Z peak", *Phys. Lett. B* **512** (2001) 30, doi:10.1016/S0370-2693(01)00690-6, arXiv:hep-ex/0106051.

[33] K. A. Olive, "Review of Particle Physics", *Chin. Phys. C* **40** (2016) 100001, doi:10.1088/1674-1137/40/10/100001.

[34] J. Alwall et al., "The automated computation of tree-level and next-to-leading order differential cross sections, and their matching to parton shower simulations", *JHEP* **07** (2014) 079, doi:10.1007/JHEP07(2014)079, arXiv:1405.0301.

[35] R. Frederix and S. Frixione, "Merging meets matching in MC@NLO", *JHEP* **12** (2012) 061, doi:10.1007/JHEP12(2012)061, arXiv:1209.6215.

[36] M. Czakon, D. Heymes, and A. Mitov, "High-precision differential predictions for top-quark pairs at the LHC", *Phys. Rev. Lett.* **116** (2016) 082003, doi:10.1103/PhysRevLett.116.082003, arXiv:1511.00549.

[37] CMS Collaboration, "Measurement of differential cross sections for top quark pair production using the lepton+jets final state in proton-proton collisions at 13 TeV", *Phys. Rev. D* **95** (2017) 092001, doi:10.1103/PhysRevD.95.092001, arXiv:1610.04191.

[38] CMS Collaboration, "Measurement of the differential cross section for $\mathrm{t\bar{t}}$ production in the dilepton final state at $\sqrt{s} = 13$ TeV", CMS Physics Analysis Summary CMS-PAS-TOP-16-011, CERN, 2016.

[39] J. R. Christiansen and P. Z. Skands, "String Formation Beyond Leading Colour", *JHEP* **08** (2015) 003, doi:10.1007/JHEP08(2015)003, arXiv:1505.01681.

[40] S. Argyropoulos and T. Sjöstrand, "Effects of color reconnection on $t\bar{t}$ final states at the LHC", *JHEP* **11** (2014) 043, doi:10.1007/JHEP11(2014)043, arXiv:1407.6653.